The Astronomical Journal, 155:153 (8pp), 2018 April https://doi.org/10.3847/1538-3881/aaaebf

The Longitudinal Evolution of Equatorial Coronal Holes

Larisza D. Krista[1,2], Scott W. McIntosh[3], and Robert J. Leamon[4,5]
[1] Cooperative Institute for Research in Environmental Sciences, University of Colorado, Boulder, CO 80309, USA;
[2] National Centers for Environmental Information, National Oceanic and Atmospheric Administration, Boulder, CO 80305, USA
[3] High Altitude Observatory, National Center for Atmospheric Research, P.O. Box 3000, Boulder, CO 80307, USA
[4] Department of Astronomy, University of Maryland, College Park, MD 20742, USA
[5] NASA Goddard Space Flight Center/ Code 672, Greenbelt, MD 20771, USA; larisza.krista@colorado.edu
Received 2017 December 21; revised 2018 February 2; accepted 2018 February 2; published 2018 March 16

Abstract

In 2011, three satellites—the *Solar-Terrestrial RElations Observatory A & B*, and the *Solar Dynamics Observatory* (*SDO*)—were in a unique spatial alignment that allowed a 360° view of the Sun. This alignment lasted until 2014, the peak of solar cycle 24. Using extreme ultraviolet images and Hovmöller diagrams, we studied the lifetimes and propagation characteristics of coronal holes (CHs) in longitude over several solar rotations. Our initial results show at least three distinct populations of "low-latitude" or "equatorial" CHs (below 65° latitude). One population rotates in retrograde direction and coincides with a group of long-lived (over sixty days) CHs in each hemisphere. These are typically located between 30° and 55°, and display velocities of ∼55 m s^{-1} slower than the local differential rotation rate. A second, smaller population of CHs rotate prograde, with velocities between ∼20 and 45 m s^{-1}. This population is also long-lived, but observed ±10° from the solar equator. A third population of CHs are short-lived (less than two solar rotations), and they appear over a wide range of latitudes (±65°) and exhibit velocities between −140 and 80 m s^{-1}. The CH "butterfly diagram" we developed shows a systematic evolution of the longer-lived holes; however, the sample is too short in time to draw conclusions about possible connections to dynamo-related phenomena. An extension of the present work to the 22 years of the combined *SOHO–SDO* archives is necessary to understand the contribution of CHs to the decadal-scale evolution of the Sun.

Key words: Sun: corona – techniques: image processing

Supporting material: animations

1. Introduction

Coronal holes (CHs) are most commonly known as individual holes in the solar corona, where the electron density and temperature is low, and the magnetic field is quasi-open, allowing solar wind to escape into the interplanetary space. In addition to being the source of high-speed solar wind and moderate geomagnetic storms, CHs are also part of the global magnetic make-up of the Sun: their location, size, and polarity demonstrates the reorganization of the global solar magnetic field over the solar cycle (e.g., Bartels 1934; Chapman & Bartels 1940; Neupert & Pizzo 1974; Wang et al. 1996; Benevolenskaya et al. 2002). These references have gone to great lengths to characterize CH lifetimes, their evolution in longitude and latitude, and their global and local magnetic connections. Indeed, there has been some observational and theoretical effort to consider whether these large, recurrent features are part of the Sun's 22-year magnetic activity cycle (e.g., Hundhausen et al. 1981; Legrand & Simon 1981; Luhmann et al. 2002). The preceding investigations, while insightful, have something in common: they were performed under the limitation of the Sun–Earth line perspective. The analysis that follows is an effort to reduce uncertainty in characterizing CH properties (for example, when considering aged data in the analysis of a "Carrington" map) by analyzing instantaneous observations of the entire solar corona.

In the present study, we use the extreme ultraviolet (EUV) observations of the entire solar corona using the twin *Solar Terrestrial Relations Observatory* (*STEREO*; Howard et al. 2008) and the *Solar Dynamics Observatory* (*SDO*; Lemen et al. 2012). When combined into a global perspective, these observations allow for the study of CH properties in a seamless fashion, where these long-lived features never disappear from view, significantly reducing uncertainty due to the feature being away from the Sun–Earth line.

The set of *SDO* and *STEREO* observations were used recently to demonstrate that magnetic activity displays behavior in space–time plots that is consistent with the presence of magnetized Rossby waves in each hemisphere McIntosh et al. (2017). Those observations illustrated that clusters of magnetic activity, as visualized through EUV brightpoints (e.g., McIntosh & Gurman 2005; McIntosh et al. 2014), exhibited westward phase and eastward group motions on the scale of tens of meters per second. These clusters also exhibited lifetimes that are, approximately, integer numbers of the rotational period at the latitudes studied. CHs are another prominent, trackable feature in the combined *SDO*/*STEREO* data set. In the following sections, we provide a brief overview of the observations used in this study, the analysis used, and a discussion of CH properties determined through the use of standard meteorological methods.

2. Observations

In the present work, we use EUV images in the 195 Å and 193 Å broadband channels taken by the *STEREO*/EUVI and *SDO*/AIA telescopes, respectively. The principal emission in these two instruments are subtly different but stem largely from Fe XII ions and so, effectively, the images carry the same information. Our intent is to study CHs without a break in longitudinal coverage, so we chose to study the timeframe from 2011 February 6 until 2014 July 1 where the images from the three spacecraft can be combined to permit our study. Furthermore, because CHs exist on rotational timescales, we

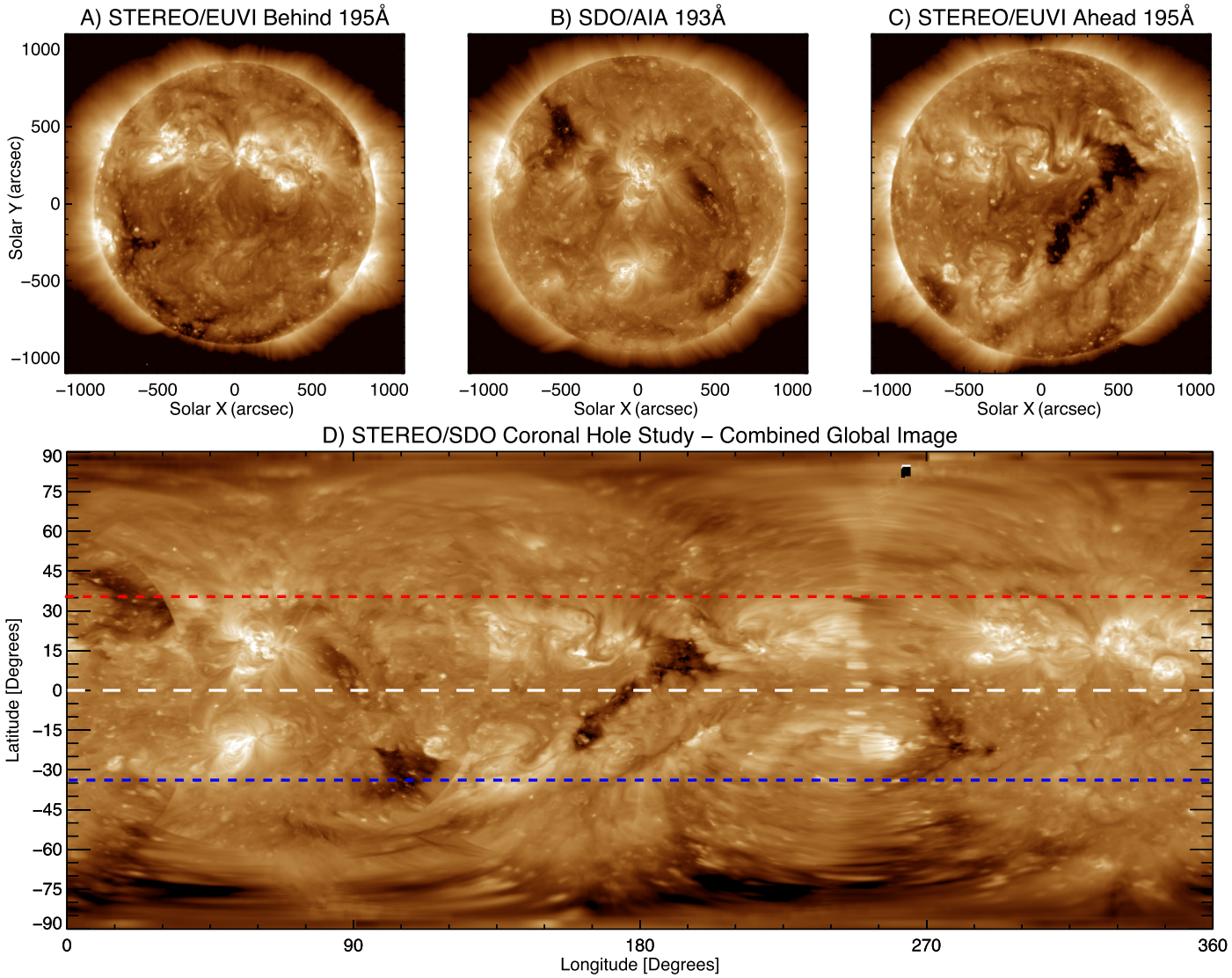

Figure 1. In the top row, from left to right, we show the *STEREO* Behind 195 Å, *SDO* AIA 193 Å, and *STEREO* Ahead 195 Å images taken at 23:45UT on 2011 August 22. The bottom row shows the combined whole coronal image as a function of heliographic longitude and latitude. In the lower panel, we show three dashed horizontal lines: at the equator (white dashed line) and at 35° in the northern and southern hemispheres (red and blue dashed lines, respectively). The electronic edition of the Journal includes an animated version of Panel (D). The animation runs from 2011 February 6 through 2014 June 30 with a cadence of 6 hr. In the animation, a white dashed line is superimposed at the equator.

(An animation of this figure is available.)

do not require the study of full-cadence observations from the observatories. Instead, we opt for a cadence of 6 hr—analyzing images occurring closest to 00:00, 06:00, 12:00, and 18:00UT.

Figure 1 shows the individual sample images (Panels (A) through (C)) from 2011 August 22 closest to 00:00UT and their combination (Panel (D)). In a straightforward process, the three individual solar images are mapped onto heliographic coordinate grids—the longitude of the image centers are prescribed by the Carrington longitude of each spacecraft. The three images are then normalized relative to their pixel intensity histograms—matching the mean of the *STEREO*/EUVI intensity histograms to that of the *SDO*/AIA image. We note that the resulting intensity histogram standard deviations match well and thus, the combined images have matching contrast. The resulting three heliographic images are superimposed onto one grid with a uniform pixel scale of 0.1°, and we simply adopt a mean value for the composite image where there is overlap between the constituent images. We note that a similar *STEREO*/*SDO* 360° image blending methodology, with a few more tweaks, was successfully carried out by Caplan et al. (2016).

3. Data Analysis

In this section, we discuss the analysis of the combined *STEREO* and *SDO* coronal imaging data that provide 360° observation of the corona. In particular, we focus on obtaining the longitudinal properties of CHs.

3.1. Hovmöller Diagrams

The analysis presented here relies on the extraction of information from Hovmöller diagrams (Hovmöller 1949). These diagrams are commonly used to plot meteorological data to highlight the role of global-scale waves in the terrestrial system. The axes of the Hovmöller diagrams are longitude (abscissa) and time (ordinate) for fixed latitudes. They are

space–time plots that illustrate the evolution of a spherical dynamical system over a range of latitudes where the resulting circular band of information represents the complete longitudinal evolution of the system with time. These diagrams have been used to illustrate the global migration of pressure ridges and seasonal rainfall migration patterns across the globe. Slanting straight lines in a Hovmöller diagram, like in any space–time plot, indicate a succession of disturbances that are propagating. The application of this meteorological method on a globally observed system can be compared to other methods that use the typical single-observing perspective. Similar analyses exploit what are known as "Bartels" plots (e.g., Chapman & Bartels 1940), or some other form of space–time plots. For further details on these methods, or resulting analyses on CH evolution, we refer to Neupert & Pizzo (1974), Wang et al. (1996), and Benevolenskaya et al. (2002).

The Hovmöller diagrams in our study were created using the 360° combined data from the *STEREO*/EUVI and *SDO*/AIA instruments (Figure 1). From the heliographic composite image set, we extract 2° wide rings at fixed latitudes. The unwrapped rings are then stacked to create a longitude–time plot. An example map is shown in Figure 2. As noted above, these diagrams are particularly useful for identifying lifetimes and the east–west drift of features relative to the differentially rotating quiet Sun (QS). The dark and bright features observed in the sequence of EUV Hovmöller diagrams show CHs and solar active regions, respectively. In this paper, we are interested in tracking the evolution of CHs, although, an analogous process to that described in the following sections could be employed to study active region propagation and lifetimes.

Figure 2 shows two sample EUV Hovmöller diagrams of the northern (Panel (A)) and southern hemispheres (Panel (B)) as illustrated by the red and blue horizontal lines shown in Figure 1 (Panel (C))—these represent coronal evolution at 35° latitude in each hemisphere. In these figures, we can clearly see that the CHs drift from right to left with time (i.e., they migrate eastward relative to the local QS). In the following section, we will discuss the method used to identify and quantify the drift signatures in the longitudinal evolution of CHs seen in the panels of Figure 2.

3.2. CH Velocity Determination

In order to derive CH characteristics (e.g., lifetime, relative velocities), we first identified the CHs in the Hovmöller diagrams by setting an intensity threshold limit. Each CH region identified was then analyzed separately to determine its properties. Note that we set a lower limit on the temporal duration of the selected regions: features that were less than 100 pixels in their extent along the y axis were excluded from the study (i.e., those with lifetimes of less than 25 days). This lifetime limit was set to minimize error in the relative velocity determination.

To obtain information about the CH contours, we divided the regions into 20 pixel segments, which is equivalent to approximately 5-day timesteps. For each segment, we identified the contour centroid (center of mass). An example of this process is shown in panel (B) of Figure 3. We then fit the segment centroids with a straight line (the blue line in panel (C)) in order to assess the east–west drift of a CH feature.

The inclination of the fitted line in the space–time plot provides the speed of the CH relative to the QS. The CH can drift eastward (left tilt, negative relative speed, retrograde drift); westward (right tilt, positive relative speed, prograde drift); or have no drift at all. In the latter case, the feature is vertical in the Hovmöller diagram and is "stationary" at that latitude (moving with the QS). Note that very few of the identified and tracked features are curved to the right or the left, as far as we can tell with the present data, i.e., few detectably accelerate or decelerate.

We analyzed the combined *STEREO*/*SDO* data set from −65° heliographic latitude to +65° in 5° steps. We identified 190 CH features between 2011 and 2014, acknowledging that most of them have latitudinal extent greater than 5°. Hence,

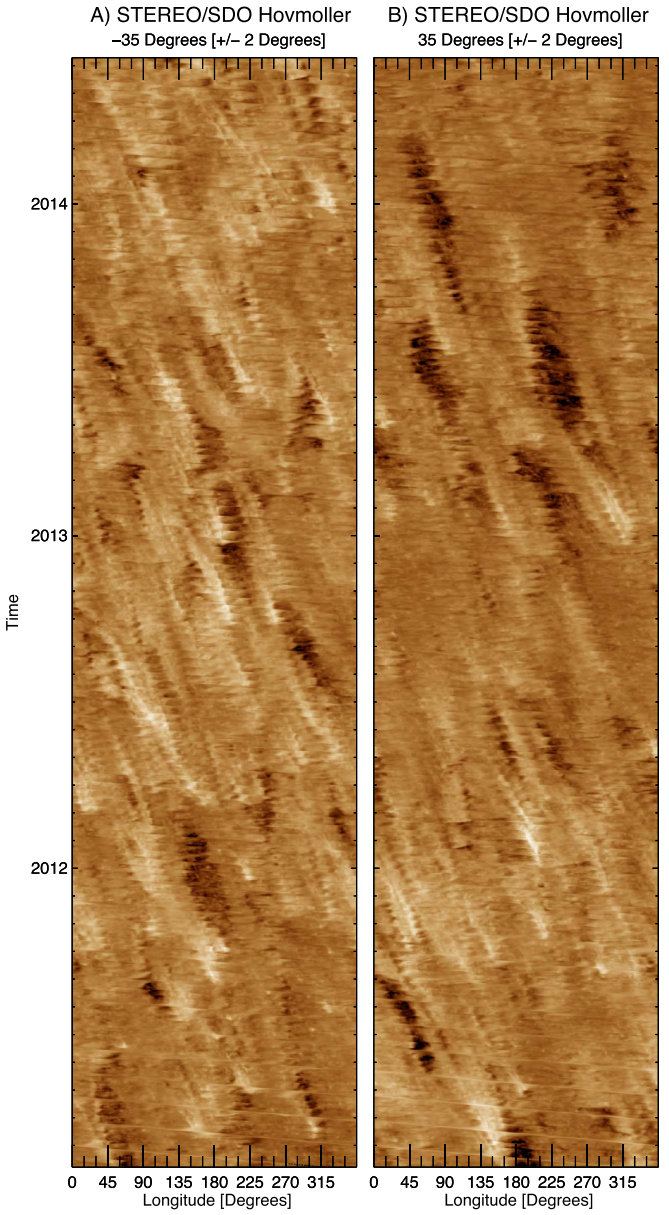

Figure 2. Hovmöller diagrams (longitude vs. time at fixed latitude) derived from the joint observations of the *STEREO*/EUVI 195 Å and *SDO*/AIA 193 Å instruments for latitudes 35° South (Panel (A)) and 35° North (Panel (B)) as shown in Figure 1. Each Hovmöller diagram is averaged over ±2° in latitude. The electronic edition of the Journal has an animated version of the scan across solar latitudes from 65° South to 65° North. (We note that time runs from bottom to top in these panels, contrary to the convention used in Bartels maps, Bartels 1934).

(An animation of this figure is available.)

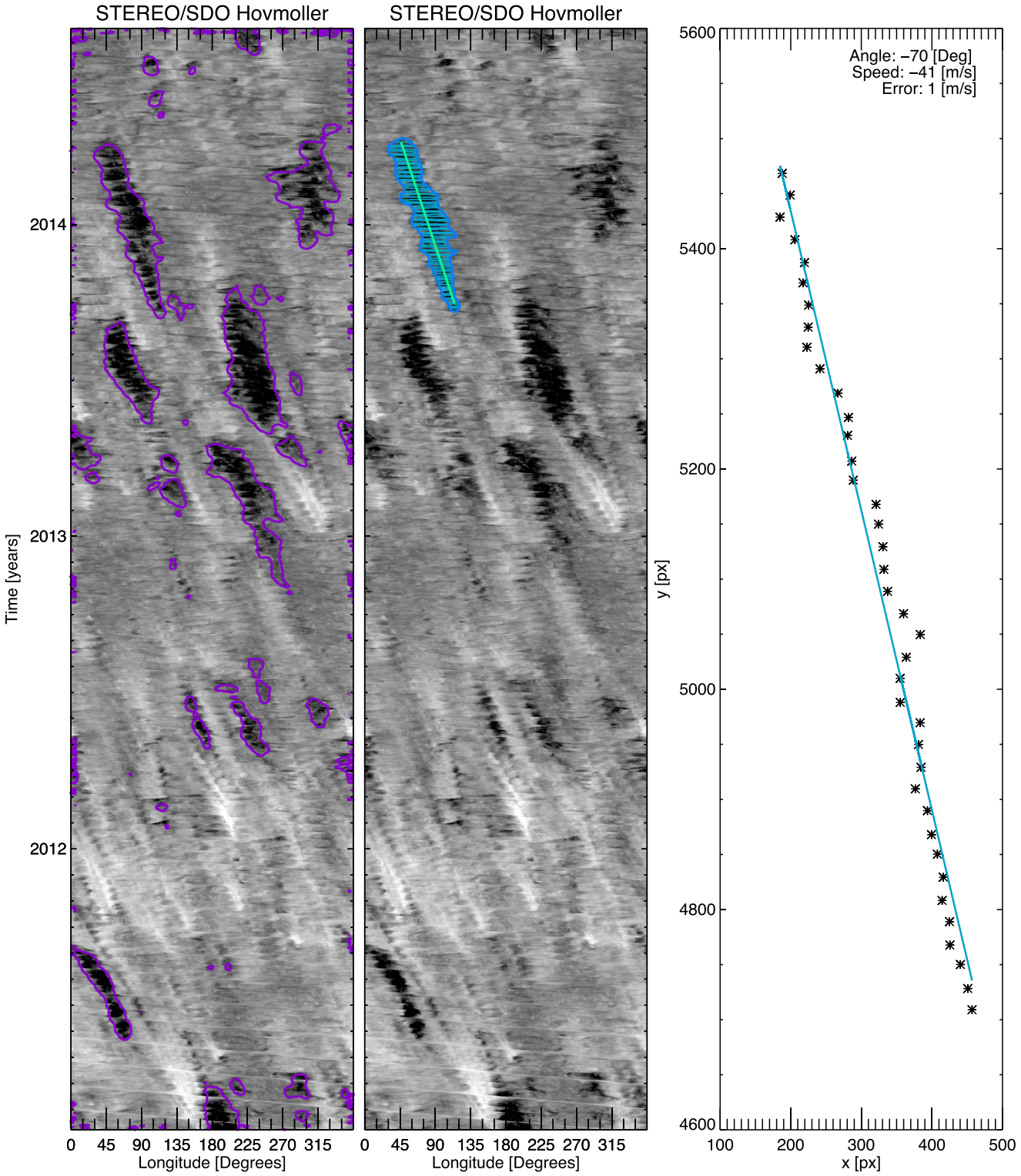

Figure 3. Panel (A) shows the *STEREO*/*SDO* Hovmöller diagram for 35° North (cf. Figure 2(B)), highlighting the detected CH boundaries in purple. Panel (B) illustrates only one CH contour that is singled out for further analysis in blue. Panel (C) shows the segment center values (black asterisks) vs. time. From these values, the best-fit line (blue straight line) was used to estimate a relative velocity of 41 (±1) m s^{-1} for the CH contour.

from the 190 CH features some are repeated observations of the same CH if it extended over a wide range of latitudes. This means that large, long-lived CHs are prominent in our study and give a good indication of the presence of persistent, large regions of open flux. From our analysis of the contours, we are able to extract information about their latitude, start ("emergence"), end ("disappearance"), lifetime, their relative drift velocity and direction, and their starting and ending longitude. Note that the period of time studied covers the complex hemispheric asymmetry of the rising phase of cycle 24 where solar maximum in the northern hemisphere was reached in late 2011 and in early 2014 for the southern hemisphere.

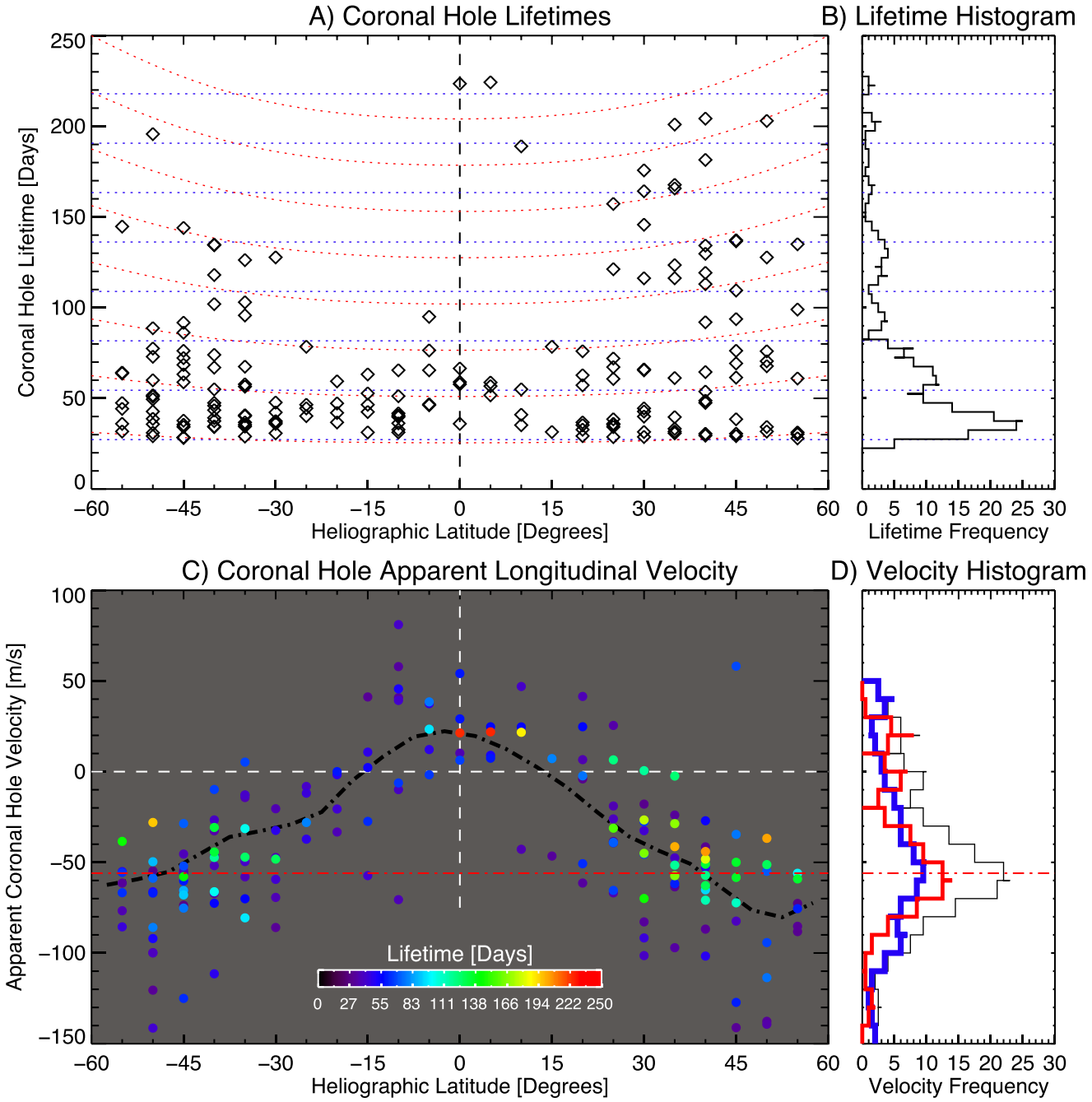

Figure 4. Panel (A) shows the distribution of CH lifetimes with latitude. We also show reference lines of constant rotational period (27.8 days and multiples thereof—blue dashed lines) and those illustrating multiples of rotational period with latitude (red dashed lines) as of Snodgrass & Ulrich (1990). Panel (B) collapses the distribution of CH lifetimes into a histogram with the 27.8-day rotational period, and multiples, shown as blue dashed lines. Panel (C) shows the distribution of relative CH velocities where the dots are colored to indicate CH lifetime. The horizontal red dashed line is drawn at velocity of 56 m s^{-1}. Panel (D) collapses the CH velocities into a single histogram (black thick line), in addition to that short-lived (<60 days) and long-lived (>60 days) CH velocities are shown as blue and red lines, respectively.

In the online animation showing the change in the Hovmöller diagrams with latitude (Figure 2), it is noticeable that true equatorial CHs (within ∼10° of the equator) are predominantly prograde—showing a definite westward inclination. Between 10° and 20° in each hemisphere, there is a mix of eastward and westward drifting CHs, but above 20° almost all CHs drift eastward—suggesting that they rotate at speeds slower than the local (differential) rotation rate. In the following section, we will quantify these visual patterns.

4. Results

Figure 4 collects the primary information derived from the 190 CH features in the 25 latitudinal bands studied without a break in observation.

The CH lifetime information is presented in panels (A) and (B) of Figure 4. In this plot, several trends are immediately visible. When considering the variation of CH feature lifetimes with latitude (Figure 4, panel (A)), there appear to be two clusters of data points: (1) a set of CHs across all latitudes with

lifetimes of less than 60 days, and (2) a set of CHs at mid-latitudes in both hemispheres and near the equator with lifetimes ranging from 60 to 250 days. Collapsing the lifetimes across latitude, we get the plot in panel (B) where it would appear that there may also be distinct groups of CH lifetimes. To explore this further, panel (A) shows two sets of curves, the blue dashed lines show integer values of 27.8 days (the approximate mean rotation rate of the solar photosphere) while the red dashed lines show the variation of rotational period with latitude as derived by Snodgrass & Ulrich (1990).

We get the visual appearance from panels (A) and (B) that the lifetimes of CHs appear to congregate around the blue and red dashed lines. This hints that those CH lifetimes are commensurate with integer numbers of the rotation rate at the corresponding latitude. Nevertheless, a larger statistical sample may be required to completely explore this connection (see below).

Panels (C) and (D) of Figure 4 show the latitudinal variation of relative velocities and lifetimes of CH features. The dots in panel (C) indicate the distribution of velocities while the dots themselves are colored by the corresponding CH feature lifetime. When velocity is considered, the previously determined two types of CHs can be further separated: the (short-lived) CHs (blue and purple dots) appear across all the latitudes sampled. However, the longer-lived CHs appear to cluster at mid-latitudes in each hemisphere with velocities of ~ -55 m s^{-1} (red dashed line), and also near the equator with velocities of ~ 20 m s^{-1}.

Computing the mean velocities of the CHs present in each latitudinal bin yields the black dotted–dashed line. This average velocity profile crosses zero apparent velocity (white dashed line) at about $\pm 18°$ latitude—this is the approximate location where the relative velocities "mix," and the prograde behavior switches to retrograde. It remains to be seen how the velocities inferred here compare to those using contemporary space–time diagnostics (e.g., Neupert & Pizzo 1974), but the numbers and behavior appear to be consistent.

The CH velocity histograms shown in panel (D) also clearly show the above described three types of CHs: short-lived CHs (>60 days; blue line) appear across all latitudes, while long-lived CHs (<60 days; red line) show a bimodal distribution, with higher frequencies at ~ -55 and ~ 20 m s^{-1}.

Figure 5 contrasts the last 22 years of sunspot activity with the short period of time where we have 360° coverage of the solar atmosphere. Using the information derived from the image series for the 190 CH features we can build a latitude versus time (or "butterfly") plot of the derived CH properties, as shown in panel (B). Each horizontal "stroke" in the butterfly diagram represents the latitude at which the CH was identified, and the start and end points in time. The color scale spans from short to long-lived. The patterns of Figure 4 can also be recognized in this figure. Equatorial CHs with long lifetimes are visible in 2012, and we can see that the longer-lived CHs in the northern hemisphere start to group in early 2013, after solar maximum, between 45°and 65° and appear to slowly migrate equatorward thereafter, an item supported by other observations (see, e.g., Figure 7 of Gibson et al. 2017). In the southern hemisphere, there are a few long-lived CHs (above 45°), but they do not appreciably show any equatorward drift in the epoch studied. Note that in the southern hemisphere, the sunspot maximum occurs very close to the end of our period of study.

5. Discussion

The alignment of the three spacecraft between 2011 and 2014 has presented us with a unique timeframe to study CHs over their entire lifespan with little ambiguity. These observations have allowed us to explore the key properties of CHs, and we identified the following:

1. There appear to be three types of CHs below 65°. The most prevalent type of CHs are short-lived (less then two solar rotations) and they appear at any latitude. Two smaller (by number) types of CHs live many solar rotations, and typically appear in both hemispheres at latitudes between 30° and 55° and also inside ±10°. Indeed, following solar maximum, in 2012, we see long-lived CHs near the equator, and in 2013 we see a cluster of persistent, long-lived CHs in the northern hemisphere that appear to migrate slowly equatorward. While there are a few long-lived CHs that appear at mid-latitudes in the southern hemisphere, no such equatorward migration is seen. However, we note that solar maximum in the southern hemisphere occurs very close to the end of our study period.
2. The distribution of CH lifetimes appears to show a dependence with the solar rotational period (with latitude). It appears that integer numbers of rotational periods are favored. This property was noticed by Ulrich (2001) and McIntosh et al. (2017) where the latter deduced that the pattern observed was a characteristic of a (magnetized) Rossby mode in the solar interior.
3. From the Hovmöller diagrams, we see that there are CHs that *do not* have active regions instantly preceding (or following) their appearance. The examples in the upper portion of Figure 2(B) are of this type—these are also long-lived CH.
4. The relative velocity distribution of CHs is complex. Below 18° latitude, most CHs exhibit prograde motions. Above 18°, we see another difference between the types of CH discussed above—the short-lived CHs can populate any latitude and have velocities that appear to become increasingly retrograde with latitude. The long-lived CHs, however, seem to exhibit uniform ~ -55 m s^{-1} velocities relative to the QS.

Unfortunately, the short span of global coverage means that we have relatively low statistics: only 190 CH features could be characterized. Ideally, we could and should exploit this timeframe to train an analysis of the 22-year *SOHO–SDO* observing epoch from the Sun–Earth line, with the acknowledgement that while statistics will increase, accuracy in lifetime will decrease. Some systematic studies of CH evolution have been undertaken (e.g., McIntosh et al. 2014; Lowder et al. 2017), but the temporal evolution of the detected CHs has not been utilized.

The long-lived, nearly uniformly rotating, mid-latitude CHs that slowly migrate equatorward after the northern hemispheric maximum have no noticeable active regions preceding them. This class, and possibly the class in the southern hemisphere too, would appear to have a connection to the global mechanics of solar evolution and not related to the breakdown of other surface features. It is interesting to place these CHs in the context of characterization of solar wind evolution (e.g., Legrand & Simon 1981), but again a longer timeframe is

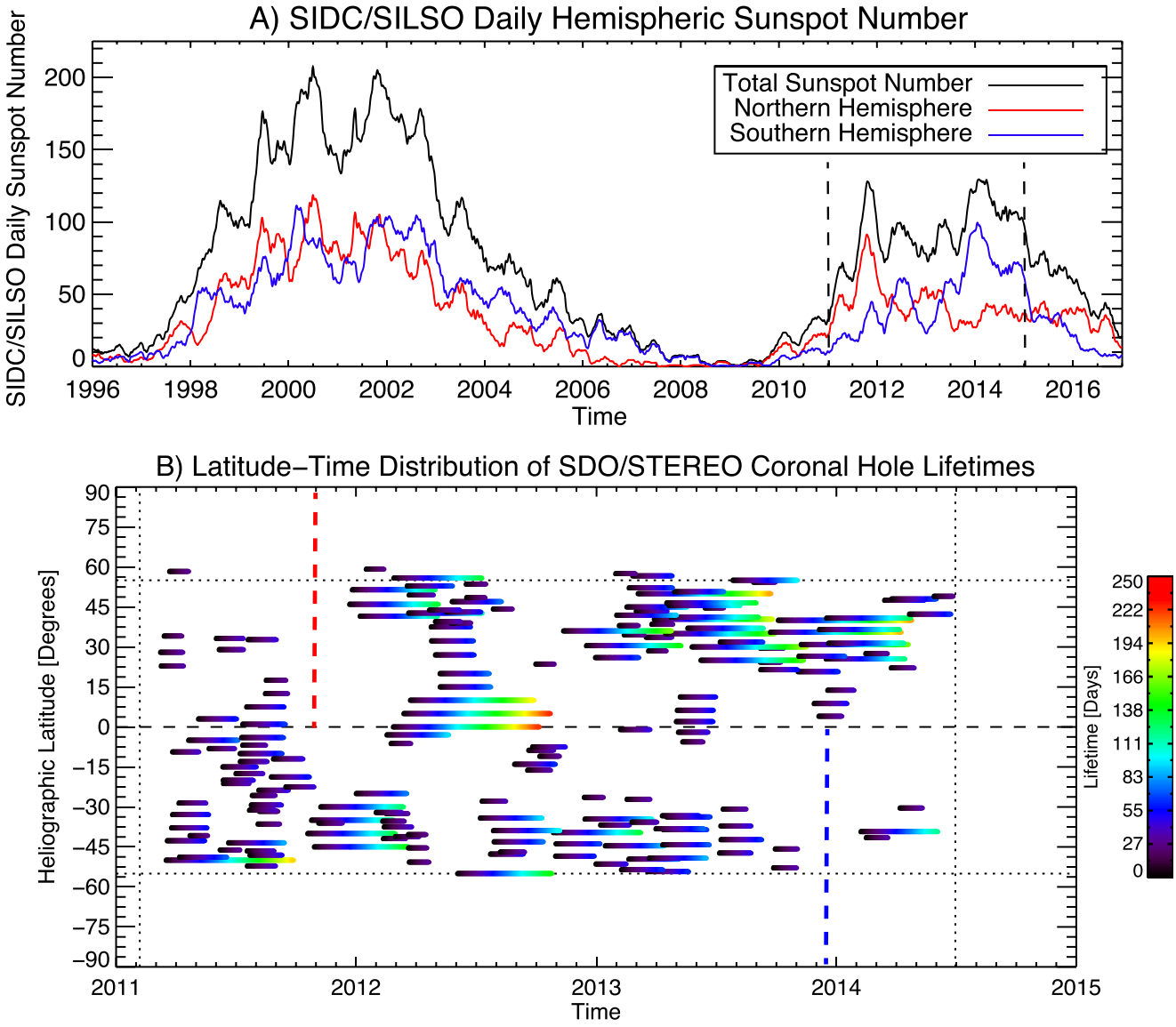

Figure 5. Panel (A) shows the evolution of the total daily (black) and hemispheric sunspot numbers over the past 22 years (northern hemisphere—red; southern hemisphere—blue) from the Solar Influences Data Center (SIDC) where the epoch studied herein is bracketed by vertical dashed black lines. The profound hemispheric asymmetry of solar cycle 24 is clearly visible. Panel (B) shows the derived CH latitude–time (or "butterfly) diagram, for the 2011–2015 epoch where we have global coverage of the EUV corona. The thick dashed red and blue lines indicate the time of sunspot maxima in the northern and southern hemispheres respectively. Panel (B) shows CH feature locations in heliographic latitude over the observation period. There are 190 CH features represented. Each is drawn as a straight line at the latitude at which it appeared, and for the duration for which it was detected. The associated lines are color-scaled to indicate the CH lifetimes, up to 250 days.

needed and one that preferably spans at least one complete 11-year sunspot cycle (e.g., Figure 7 of Cranmer et al. 2017).

There are clear signatures of rotational modulation in our analysis of CH lifetimes. This is highlighted by the presence of CH lifetimes that are an integer number of the rotational period at the latitude they are being studied and is most clearly observed in long-lived CHs. As noted above, this property has been linked to deep-rooted rotationally driven Rossby modes present on the magnetic activity bands that make up the 22-year solar magnetic activity cycle (McIntosh et al. 2017). We might not expect to see such a relationship for a structure that has its roots shallow in the solar interior, or photosphere, because the convective forces (with timescales of minutes to a couple of days) would slowly erode said structure over the order of a rotation. That being said, there are many CHs in our sample—particularly those with shorter lifetimes—that could be subject to the latter formation and erosion process. Such an investigation is beyond the scope of this article and could be the subject of future investigation: comparing contemporary and "meteorological" approaches to the 22 years of high-quality *SOHO*, *STEREO*, and *SDO* EUV observations of the corona and CHs.

6. Conclusion

Our main results show that CHs below 65° latitude (also commonly known as equatorial CHs) are not all the same. There appears to be at least three previously unidentified classes of CHs that are defined by their clustering locations, lifetimes, and prograde or retrograde rotational tendencies. Although the total number of CH features in our current sample is small, a carefully linked study of the last 22 years of EUV

observations from the Sun–Earth line may link long-lived CHs to a branch of the solar dynamo.

L.D.K. was supported by the National Aeronautics and Space Administration under grant No. NNX15AB91G, issued through the NASA/LWS Program. NCAR is sponsored by the National Science Foundation. Data from the *STEREO* and *SDO* spacecraft are openly available from the respective mission archives.

ORCID iDs

Larisza D. Krista https://orcid.org/0000-0003-4627-8967
Scott W. McIntosh https://orcid.org/0000-0002-7369-1776
Robert J. Leamon https://orcid.org/0000-0002-6811-5862

References

Bartels, J. 1934, TeMAE, 39, 201
Benevolenskaya, E. E., Kosovichev, A. G., & Scherrer, P. H. 2002, AdSpR, 29, 389
Caplan, R. M., Downs, C., & Linker, J. A. 2016, ApJ, 823, 53
Chapman, S., & Bartels, J. 1940, in Geomagnetism, Vol. I: Geomagnetic and Related Phenomena, ed. S. Chapman & J. Bartels (Oxford Univ. Press: London)
Cranmer, S. R., Gibson, S. E., & Riley, P. 2017, SSRv, arXiv:1708.07169
Gibson, S. E., Webb, D., Hewins, I. M., et al. 2017, in IAU Symp. 328, Living Around Active Stars, ed. D. Nandy, A. Valio, & P. Petit (Cambridge: Cambridge Univ. Press), 93
Hovmöller, E. 1949, Tell, 1, 62
Howard, R. A., Moses, J. D., Vourlidas, A., et al. 2008, SSRv, 136, 67
Hundhausen, A. J., Hansen, R. T., & Hansen, S. F. 1981, JGR, 86, 2079
Legrand, J. P., & Simon, P. A. 1981, SoPh, 70, 173
Lemen, J. R., Title, A. M., Akin, D. J., et al. 2012, SoPh, 275, 17
Lowder, C., Qiu, J., & Leamon, R. 2017, SoPh, 292, 18
Luhmann, J. G., Li, Y., Arge, C. N., Gazis, P. R., & Ulrich, R. 2002, JGRA, 107, 1154
McIntosh, S. W., Cramer, W. J., Pichardo Marcano, M., & Leamon, R. J. 2017, NatAs, 1, 0086
McIntosh, S. W., & Gurman, J. B. 2005, SoPh, 228, 285
McIntosh, S. W., Wang, X., Leamon, R. J., et al. 2014, ApJ, 792, 12
Neupert, W. M., & Pizzo, V. 1974, JGR, 79, 3701
Snodgrass, H. B., & Ulrich, R. K. 1990, ApJ, 351, 309
Ulrich, R. K. 2001, ApJ, 560, 466
Wang, Y.-M., Hawley, S. H., & Sheeley, N. R., Jr. 1996, Sci, 271, 464